Langmuir

ARTICLE

pubs.acs.org/Langmuir

Interaction between Brush Layers of Bottle-Brush Polyelectrolytes: Molecular Dynamics Simulations

Daniel Russano, Jan-Michael Y. Carrillo, and Andrey V. Dobrynin*

Polymer Program, Institute of Materials Science and Department of Physics, University of Connecticut, Storrs, Connecticut 06269, United States

ABSTRACT: Interactions between tethered layers composed of aggrecan (charged bottle-brush) macromolecules are responsible for the molecular origin of cartilage biomechanical behavior. To elucidate the role of the electrostatic forces in interaction between bottle-brush layers, we have performed molecular dynamics simulations of charged and neutral bottle-brush macromolecules tethered to substrates. In the case of charged bottle-brush layers, the disjoining pressure P between two brush layers in salt-free solutions increases with decreasing distance D between substrates as $P \propto D^{-1.8}$. A stronger dependence of the disjoining pressure P on the surface separation D was observed for neutral bottle-brushes, $P \propto D^{-4.6}$, in the same interval of disjoining pressures. These scaling laws for dependence of disjoining pressure P on distance D are due to bending energy of the bottle-brush macromolecules within compressed brush layers. The weaker distance dependence observed in polyelectrolyte bottle-brushes is due to interaction between counterion clouds surrounding the bottle-brush macromolecules preventing strong brush overlap.

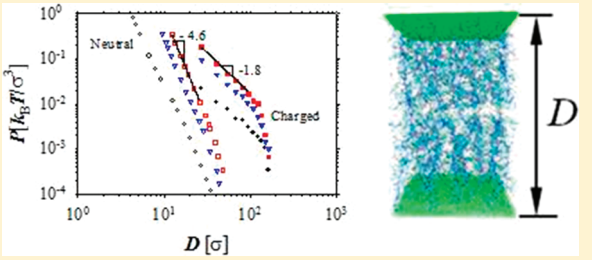

1. INTRODUCTION

Brush layers of tethered polyelectrolyte chains have attracted considerable attention during the past two decades.[1−10] Experimental,[1,3,5,9] theoretical,[11−15] and computational[16−22] studies of polyelectrolyte brushes have shown that electrostatic interactions between ionized groups and salt ions are the main factor responsible for the unique properties of this class of polymeric systems. The brush properties depend on the fraction of charged monomers on the polymer backbone, pH and ionic strength of the solutions, polymer grafting density, and polymer−solvent affinity. At low salt concentrations, the strong electrostatic interactions between ionized groups and counterions result in counterion condensation inside the brush, almost neutralizing the brush layer. In this regime the deformation of the grafted polyelectrolyte chains is caused by the osmotic pressure of counterions localized within the brush. This counterion osmotic force is balanced by the chain's elastic energy. The unique feature of this so-called "osmotic brush" regime is that the thickness of the brush layer shows only a weak dependence on the brush grafting density.[1,3] Addition of salt leads to screening of the electrostatic interactions inside the brush such that, at sufficiently high salt concentrations, the properties of the polyelectrolyte brush become similar to those of the neutral brushes, with the effective monomer−monomer second virial coefficient determined by the local salt concentration. At high salt concentrations, the thickness of the planar polyelectrolyte brush decreases with increasing salt concentration as $c_s^{-1/3}$.[3,9] The solvent quality for the polymer backbone plays an important role in controlling the brush morphology. In poor solvent conditions for the polymer backbone, polyelectrolyte chains forming a brush could be in the necklacelike conformation, form a dense polymeric layer, or self-assemble into pinned spherical or cylindrical micelles. These different brush morphologies optimize the electrostatic interaction between ionized groups, counterion configurational entropy, and solvophobic interactions between polymer and surrounding solvent.[23−25] The transition between different brush morphologies can be induced by changing solution pH, fraction of charged monomers on the polymer backbone, and temperature.

The polyelectrolyte brush layers begin to interact with each other at distances D larger than their combined thickness $2H$. At these separations, $D > 2H$, two brush layers interact with each other through electrical double layers extended beyond the edge of the brush.[5] Computer simulations[18] of interaction between two polyelectrolyte brushes in salt-free solutions showed that the magnitude of the disjoining pressure (interaction force between substrates per unit area) P is inversely proportional to the substrate separation $P \propto D^{-1}$. In this regime the interaction between brushes can result in chain contraction, which is manifested as a decrease in layer thickness with decreasing brush separation.[18,19] For overlapping brush layers, $D < 2H$, the interaction between polyelectrolyte brushes depends on salt concentration. In the osmotic brush regime, when counterions are localized within the brush layer, the repulsion between brushes is dominated by the osmotic pressure of these counterions. In this regime the disjoining pressure between brush layers increases as $P \propto D^{-1}$.[12,13,15] At high salt concentrations, when

Received: May 13, 2011
Revised: July 12, 2011
Published: August 02, 2011

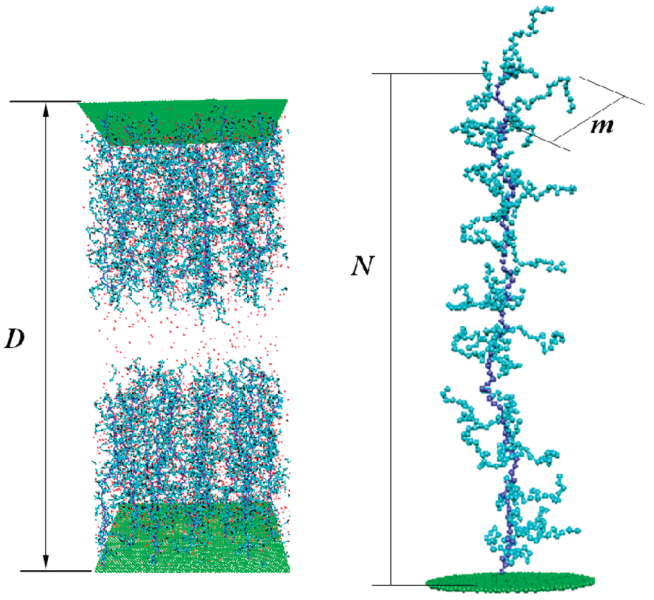

Figure 1. Snapshot of the simulation box and bottle-brush macromolecule.

Donnan equilibrium controls the concentration of salt ions within brush layers, the disjoining pressure between brushes shows faster increase with separation, $P \propto D^{-2}$. In salt-free solutions at moderate brush compressions, short-range monomer−monomer interactions start to dominate the interactions between highly overlapping chains. In this regime the disjoining pressure scales with surface separation as $P \propto D^{-2}$.[18] Note that under θ solvent conditions for the polymer backbone the disjoining pressure is inversely proportional to the third power of the distance between substrates, D^{-3}.[18] Finally, at high brush compressions, the excluded volume interactions result in even stronger dependence of disjoining pressure on substrate separation.

Electrostatic interactions are believed to be responsible for the unique lubricating properties of polyelectrolyte brushes.[6,7,26−30] It was shown that brushlike polyelectrolyte layers consisting of glycoproteins, in which large numbers of sugar chains are bound along the polymer backbone (bottle-brush polyelectrolytes), display the fascinating low-friction properties of biological connective tissues such as cartilage.[29] The cartilages of mammalian joints have remarkably low friction coefficients in the range 0.001−0.03 and can withstand pressures on the order of tens of atmospheres and shear rates from low values up to 10^6 s^{-1}.[29,31−33] Synthetic polymeric systems can also demonstrate properties similar to biological substrates.[6,28,30,34] Force measurements[6,28] between hydrophobized mica surfaces covered with hydrophobic−polyelectrolyte diblock copolymers [poly(methyl methacrylate)−poly(sodium sulfonated glycidyl methacrylate)] have shown that these substrates have excellent lubricating properties with quality approaching physiologically relevant limits. The extremely low friction between polyelectrolyte layers was attributed to the osmotic pressure of free counterions, which suppressed the layer interpenetration.[29]

In this paper we present the results of molecular dynamics simulations and a scaling analysis of interactions between two bottle-brush layers (see Figure 1). We performed simulations of neutral and charged bottle-brush layers at different brush grafting densities and different magnitudes of the compression force. By comparing the results of molecular dynamics simulations of neutral and charged bottle-brushes, we demonstrated what effect the osmotic pressure of counterions localized between and within two bottle-brush layers has on the brush interactions.

2. SIMULATION DETAILS

We performed molecular dynamics (MD) simulations[35,36] of interaction between grafted layers of charged bottle-brush macromolecules with explicit counterions. Polyelectrolyte bottle-brush macromolecules were modeled by chains of charged Lennard-Jones (LJ) particles (beads) with diameter σ. The bottle-brush macromolecules consisted of a main chain with degree of polymerization $N = 97$ and side chains with degree of polymerization $m = 21$ (see Figure 1). (The bottle-brush model is similar to the one used in our simulations of bottle-brush layers.[37]) There were a total of $N_m = 31$ side chains per each bottle-brush macromolecule, which corresponds to every third monomer of the main chain having a side chain attached to it. Only side chains were charged, with the fraction of charged monomers $f = {}^1/_3$ corresponding to every third monomer carrying a negative electrical charge, −e. The number N_B of bottle-brush macromolecules was grafted to a substrate. There were two substrates per simulation box located at $z = 0$ and $z = D$ (see Figure 1). Each substrate was modeled by a periodic hexagonal packed lattice of beads composed of 80 × 70 beads with diameter σ. The brush grafting density of the substrate, ρ_g, was equal to 1.24×10^{-3} σ^{-2}, 3.09×10^{-3} σ^{-2}, and 4.43×10^{-3} σ^{-2}. The system dimensions in the xy-plane were $70.0\sigma \times 69.28\sigma$.

All particles in the system interacted through truncated-shifted Lennard-Jones (LJ) potential:

$$U_{LJ}(r_{ij}) = \begin{cases} 4\varepsilon_{LJ}\left[\left(\frac{\sigma}{r_{ij}}\right)^{12} - \left(\frac{\sigma}{r_{ij}}\right)^{6} - \left(\frac{\sigma}{r_{cut}}\right)^{12} + \left(\frac{\sigma}{r_{cut}}\right)^{6}\right] & r \le r_{cut} \\ 0 & r > r_{cut} \end{cases} \quad (1)$$

where r_{ij} is the distance between ith and jth beads and σ is the bead diameter, chosen to be the same regardless of the bead type. The cutoff distance $r_{cut} = 2.5\sigma$, was chosen for polymer−polymer interactions, and $r_{cut} = 2^{1/6}\sigma$ was chosen for all other pairwise interactions. The interaction parameter ε_{LJ} was equal to k_BT for polymer−counterion, counterion−counterion, polymer−substrate, and counterion−substrate interactions, where k_B is the Boltzmann constant and T is the absolute temperature. The value of the Lennard-Jones interaction parameter for the polymer−polymer pair was set to $0.3k_BT$, which is close to a θ solvent condition for the polymer backbone. By selecting the strength of the polymer−polymer interactions close to the θ point, we minimized the effect of short-range interactions on the bottle-brush properties.

The connectivity of monomers into bottle-brush macromolecules was maintained by the finite extension nonlinear elastic (FENE) potential:

$$U_{FENE}(r) = -\frac{1}{2} k_{spring} R_{max}^2 \ln\left(1 - \frac{r^2}{R_{max}^2}\right) \quad (2)$$

with spring constant $k_{spring} = 30k_BT/\sigma^2$ and maximum bond length $R_{max} = 1.5\sigma$. The repulsive part of the bond potential was represented by the truncated-shifted LJ potentials with $\varepsilon_{LJ} = k_BT$ and $r_{cut} = 2^{1/6}\sigma$.

Interaction between any two charged particles with charge valences q_i and q_j, separated by a distance r_{ij}, was given by the Coulomb potential:

$$U_{Coul}(r_{ij}) = k_BT \frac{l_B q_i q_j}{r_{ij}} \quad (3)$$

where $l_B = e^2/\varepsilon k_BT$ is the Bjerrum length, defined as the length scale at which the Coulomb interaction between two elementary charges e, in a dielectric medium with dielectric constant ε, is equal to the thermal

energy k_BT. In our simulations, the value of the Bjerrum length l_B was equal to 1.0σ.

The particle−particle particle−mesh (PPPM) method implemented in LAMMPS[36] with the sixth-order charge interpolation scheme and estimated accuracy 10^{-5} was used for calculations of the electrostatic interactions between all charges in the system. The 2D periodic images of the system were periodically replicated along the z-direction with distance $L = 3D$ between their boundaries. This reduced the problem of calculation of the electrostatic interactions in a 2D periodic system to those in a 3D system.

We performed simulations that modeled compression of the bottle-brush layers. In these simulations the location of both substrates was fixed (see Figure 1). To maintain a constant temperature, the system was coupled to a Langevin thermostat. In this case, the equation of motion of the ith particle was

$$m\frac{\mathrm{d}\vec{v}_i(t)}{\mathrm{d}t} = \vec{F}_i(t) - \xi\vec{v}_i(t) + \vec{F}_i^{\,R}(t) \quad (4)$$

where $\vec{v}_i(t)$ is particle velocity and $\vec{F}_i(t)$ is the net deterministic force acting on the ith particle of mass m. $\vec{F}_i^{\,R}(t)$ is the stochastic force acting on a particle that has zero average value, $\langle\vec{F}_i^{\,R}(t)\rangle = 0$, and δ-functional correlations $\langle\vec{F}_i^{\,R}(t)\cdot\vec{F}_i^{\,R}(t')\rangle = 6\xi k_BT\delta(t-t')$. The friction coefficient ξ was set to $\xi = 0.143m/\tau_{LJ}$, where τ_{LJ} is the standard LJ time, $\tau_{LJ} = \sigma(m/\varepsilon_{LJ})^{1/2}$. The velocity−Verlet algorithm with a time step $\Delta t = 0.01\tau_{LJ}$ was used for integration of the equations of motion (eq 4).

Simulations were performed via the following procedure: at the beginning of each simulation run, the main and side chains of the bottle-brush macromolecules were in fully extended conformation with the main chain pointing along the z-directions and side chains were randomly oriented in the xy-plane. A similar substrate was placed at $z = 198\sigma$ with the brush layer pointing toward the bottom substrate (see Figure 1). Neutralizing monovalent counterions were uniformly distributed over the volume of the simulation box. A system was compressed to desired D by moving a top substrate and rescaling the simulation box. After that a system was equilibrated for 5×10^5 MD steps with electrostatic interactions turned off and for an additional 10^6 MD steps with electrostatic interactions turned on. This was followed by the production run lasting 10^6 MD steps. There were 2000 data sets collected during the production run.

To elucidate the role of electrostatic interactions on the interaction between brush layers, we have performed simulations of neutral bottle-brush layers consisting of bottle-brush macromolecules with degree of polymerization of the side chains, $m = 21$, in the same range as the brush grafting densities. The parameters for bond potential and Lennard-Jones interaction potentials were the same as in the case of the charged bottle-brush macromolecules. The total duration of the simulation runs for these systems was 4×10^6 MD steps and the last 2×10^6 MD steps were used for the data analysis. We have collected 4000 data sets during production run.

The duration of the simulation runs was optimized in such a way to allow the average force acting on the substrate beads to saturate. In Figure 2a we show evolution of the repulsion force acting on the substrate beads averaged over all beads during the simulation run. The red line corresponds to force acting on a substrate bead averaged within a time interval $\Delta\tau = 10^3\tau_{LJ}$.

We have also performed simulations of brush compression by applying a force f_z pointing toward the bottom substrate to each bead forming a top substrate. For constant force simulations to maintain a constant temperature, we have applied the Langevin thermostat in the xy-plane only. The initial box size along z-direction was set to $L_z = 200\sigma$. This box size was used to set up a grid for PPPM calculations of the electrostatic interactions. In these simulations we have measured an average separation between substrates $\langle D\rangle$ as a function of the compression force acting on the top substrate. The force-separation curves

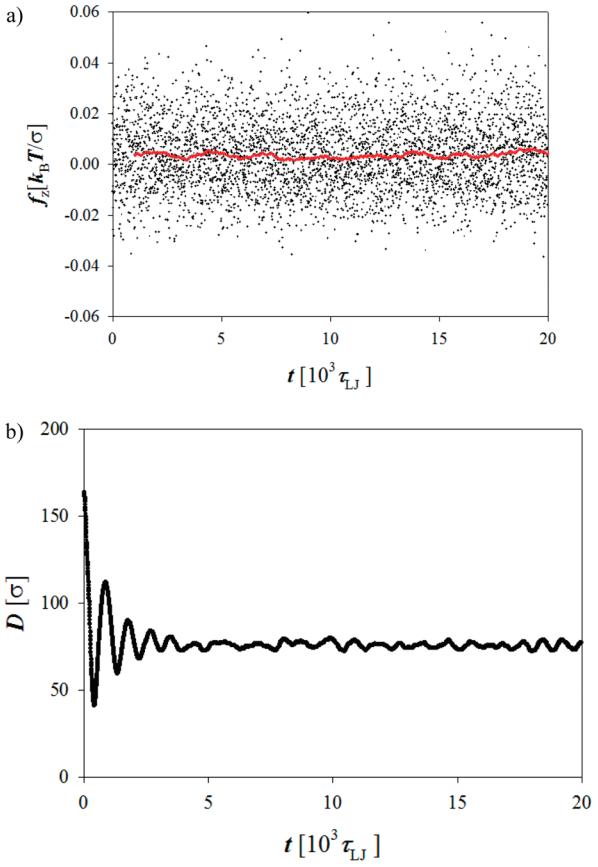

Figure 2. (a) Time evolution of the average repulsion force acting on the substrate beads obtained during simulation run of the charged bottle-brush system with distance between substrates $D = 81.53\sigma$ and brush grafting density $\rho_g = 1.24 \times 10^{-3}\ \sigma^{-2}$. The red line correspond to time-averaged force within time window $\Delta\tau = 10^3\tau_{LJ}$. (b) Time evolution of the distance between substrates obtained during the simulation run of the charged bottle-brush system with brush grafting density $\rho_g = 1.24 \times 10^{-3}\ \sigma^{-2}$ and compression force $f_z = 3.725 \times 10^{-3}\ k_BT/\sigma$ acting on each bead of the top substrate.

obtained from both simulations are within statistical error from each other. The duration of the simulation runs was the same as in the case of the constant substrate separation simulations. Figure 2b illustrates evolution of the distance between substrates D during a simulation run.

3. SIMULATION RESULTS

Figure 3 shows dependence of the disjoining pressure between substrates on the distance between substrates D. The values of the disjoining pressure for this figure were obtained by dividing a magnitude of average force f_z acting on each bead of the substrate by area per bead ($a_0 = 0.866\sigma^2$), that is, $P = f_z/a_0$ for constant D simulations. In constant compression force simulations at equilibrium, the magnitude of the disjoining pressure is equal to the magnitude of the compression force per unit area. It follows from this figure that neutral and charged bottle-brushes behave qualitatively differently. Charged bottle-brush layers begin to interact before two layers come into physical contact with each other (see Figure 4 A). This interaction is caused by the diffusive counterion clouds that escape the brush interior. At separations D larger than the combined average brush thickness $2H$, the interaction between two brush layers is identical to the

dx.doi.org/10.1021/la2018067 |Langmuir 2011, 27, 11044–11051

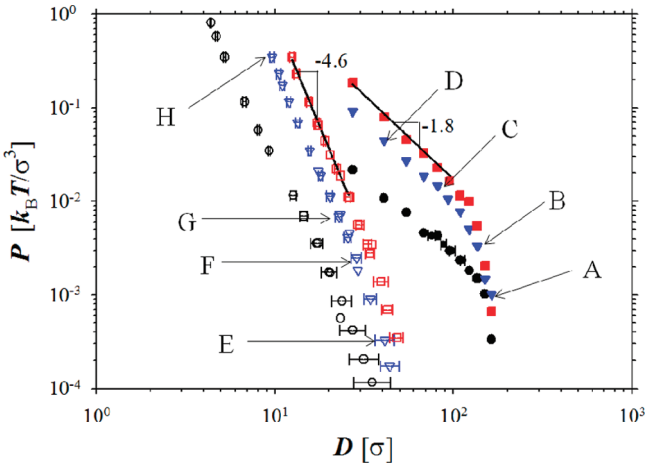

Figure 3. Dependence of disjoining pressure on distance D between substrates for neutral (open symbols) and charged (solid symbols) bottle-brush layers at different brush grafting densities: (○, ●) ρ_g = 1.24 × 10^{-3} σ^{-2}, (▽, ▼) ρ_g = 3.09 × 10^{-3} σ^{-2}, and (□, ■) ρ_g = 4.43 × 10^{-3} σ^{-2}. Snapshots of the brush layer conformations corresponding to letters A−H are shown in Figure 4. Data points with horizontal error bars correspond to constant compression force simulations.

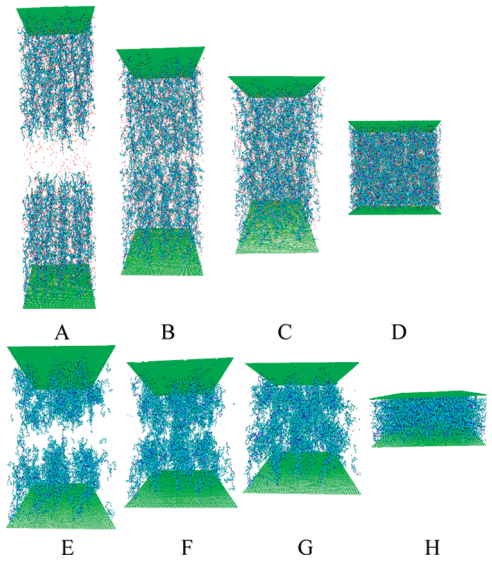

Figure 4. Snapshots of bottle-brush layers at different compressions.

interaction between two charged substrate separated by a distance $D - 2H$ and carrying the effective surface charge density Σ. Localized within the bottle-brush layer counterions reduce an effective surface charge density of the brush layer to $\Sigma = (1 - x_H)\rho_g fmN_m$, where x_H is the fraction of counterions localized within brush layer. For the remaining outside brush counterions, their density distribution is given by[38]

$$\rho_c(z) = \frac{\rho_0}{\cos^2[s(z - D/2)]} \quad (5)$$

where ρ_0 is the counterion concentration at the middle plane separating two brush layers, and the parameter s is a root of the nonlinear equation $s \tan[s(D/2 - H)] = 2\pi l_B \Sigma$.[38] Note that eq 5 is a solution of the nonlinear Poisson−Boltzmann equation,

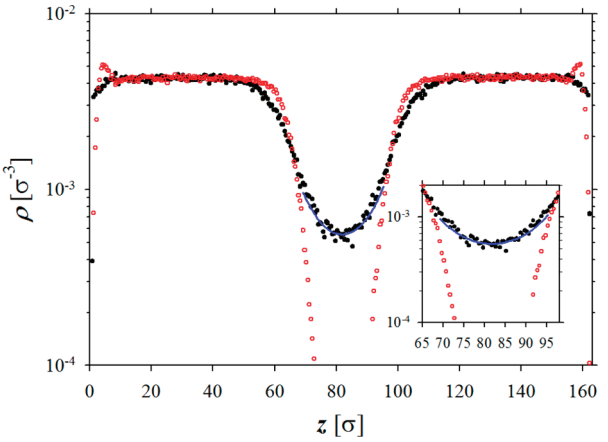

Figure 5. Distribution of charged monomers of the bottle-brush (red circles) and counterions (black circles) for bottle-brush layers with brush grafting density ρ_g = 1.24 × 10^{-3} σ^{-2} and distance between substrates $D = 163\sigma$. The line corresponds to eq 5 with value of the parameter s = 5.61 × 10^{-2} σ^{-1}.

which couples distribution of counterions with electrostatic potential (see for details ref 38). The disjoining pressure in this regime is equal to[38]

$$P = k_B T \rho_0 = k_B T \frac{s^2}{2\pi l_B} \quad (6)$$

In Figure 5 we have verified how well eq 5 describes the distribution of counterions outside the brush. The parameter s for this plot was obtained by solving a nonlinear equation relating the parameter s to the effective surface charge density Σ and the thickness of the bottle-brush layer H. For this plot we selected the brush thickness to be equal to $H = 69.25\sigma$, which corresponds to density of charged monomers ρ_f = 5 × 10^{-3} σ^{-3}. For this brush layer thickness the effective surface charge number density is Σ = 7.6 × 10^{-3} σ^{-2} and value of the parameter s = 5.61 × 10^{-2} σ^{-1}. As one can see, the agreement between eq 5 and the result of the computer simulation is very good. It follows from Figure 5 that, inside the brush layers, counterions almost completely neutralize the brush charge. The excess charge of the bottle-brush layer is located close to the edge of the brush layer. This charge distribution throughout the brush-layer thickness minimizes the total electrostatic energy stored within the brush layers. The excess charge of the bottle-brush layer is compensated by the diffusive layer of counterions filling the space between two brush layers. Further corroboration of applicability of the Poisson−Boltzmann approach to describe counterion distribution between brush layers comes from Figure 6, which shows a linear relationship between disjoining pressure and counterion density at the middle plane as predicted by eq 6. Thus, at these separations the counterion clouds between brush layers dominate the screening of the excess charge of brush layers and the interaction between them. A similar effect was observed in simulations of the brushes made of linear chains (see for review refs 1−3).

The crossover to a new universal regime occurs when two bottle-brush layers come into contact. In this new regime, the disjoining pressure increases with decreasing distance between substrates as $D^{-1.8}$. Note that this power law dependence is observed for all our charged bottle-brush systems independent of

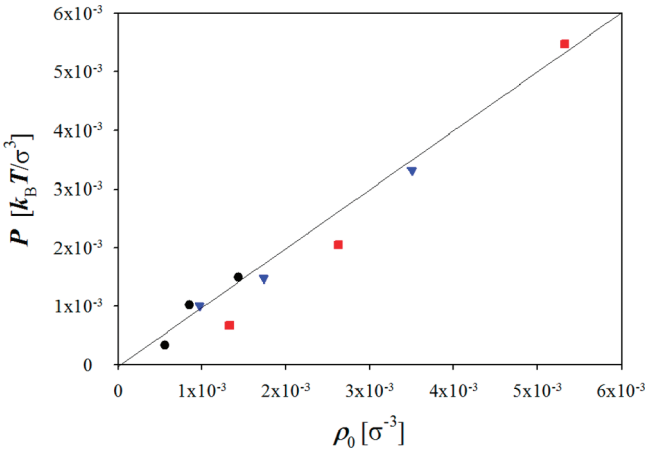

Figure 6. Dependence of disjoining pressure P on counterion density ρ_0 at the middle plane between two bottle-brush layers for different brush grafting densities: (●) $\rho_g = 1.24 \times 10^{-3}\ \sigma^{-2}$, (▼) $\rho_g = 3.09 \times 10^{-3}\ \sigma^{-2}$, and (■) $\rho_g = 4.43 \times 10^{-3}\ \sigma^{-2}$.

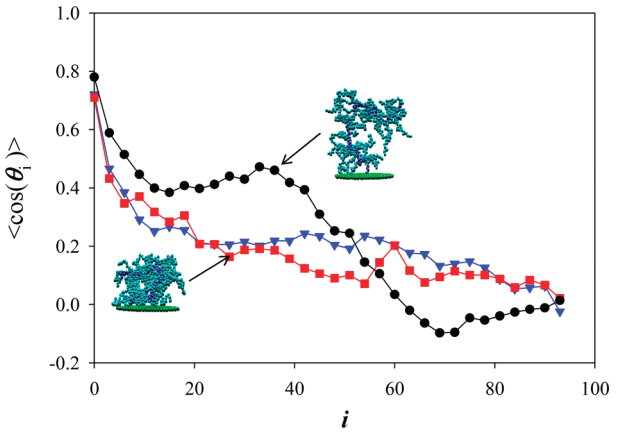

Figure 7. Variation of the average cosine $\langle \cos(\theta_i) \rangle$ along backbone of the charged-bottle brush macromolecules at substrate separation $D = 27.2\sigma$ and different brush grafting densities: (●) $\rho_g = 1.24 \times 10^{-3}\ \sigma^{-2}$, (▼) $\rho_g = 3.09 \times 10^{-3}\ \sigma^{-2}$, and (■) $\rho_g = 4.43 \times 10^{-3}\ \sigma^{-2}$. Insets show typical bottle-brush configurations.

the brush grafting density. Differences in brush grafting density result in parallel shifts of the interaction curves with respect to each other. The strength of the interaction between bottle-brush layers monotonically increases with increasing brush grafting density. It is also interesting to point out that despite the significant change in the brush conformations seen in Figures 4 C and D, the power law dependence of the disjoining pressure does not change. It is worth pointing out that, for the lowest brush grafting density, $\rho_g = 1.24 \times 10^{-3}\ \sigma^{-2}$, there is a shoulder in the disjoining pressure dependence on the substrate separation located at $D \sim 90\sigma$ (see Figure 3). This shoulder disappears with increasing brush grafting density.

In the overlapping brush regime, in addition to the counterion osmotic pressure, the interactions between bottle-brushes contribute to the net repulsive force between substrates. As two bottle-brush layers start to overlap the bottle-brush macromolecules begin to bend, providing an additional bending energy contribution to the interaction energy. To illustrate the bending of the bottle-brush macromolecules in Figure 7 we show

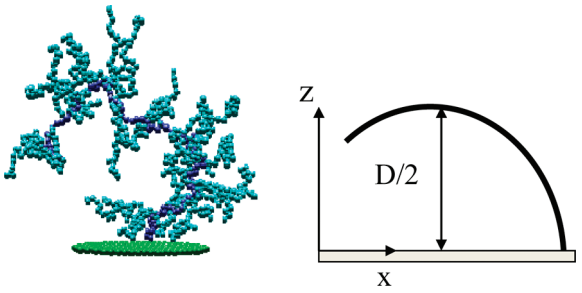

Figure 8. (Left) Snapshot of the typical bottle-brush configuration in the compressed layer and (right) approximation of the bottle-brush backbone by an arch for estimation of the bottle-brush bending energy.

dependence of the average cosine between a normal vector to the substrate and a radius vector connecting every third bead along the bottle-brush backbone at different brush grafting densities. At low brush grafting densities the average value of the cosine can become negative indicating the turning point of the bottle-brush backbone. For larger brush grafting densities the value of the cosine approaches zero toward the end of the bottle-brush backbone. Thus, the end of the bottle-brush macromolecule is aligned parallel to the substrates.

To estimate a bending energy contribution to the bottle-brush free energy, we will assume that the brush is bent in the xz-plane (see Figure 8). The configuration of the bottle-brush macromolecule in this regime can be characterized by a set of the unit vectors $\vec{n}(l) = [n_x(l), n_z(l)]$ describing the orientation of the bottle-brush backbone in the deformation plane where l is a curvilinear coordinate along the brush backbone varying between 0 and $L \approx Nb$, where b is the average bond length of the backbone. The orientation of the unit vectors $\vec{n}(l)$ is convenient to describe in terms of an angle, $\theta(l)$, that this vector makes with the z axis, $\vec{n}(l) = (\sin[\theta(l)], \cos[\theta(l)])$ (see Figure 8). The brush bending energy is written as follows:[39]

$$\frac{U_{\text{bend}}}{k_B T} = \frac{l_p}{2}\int_0^L \left(\frac{\mathrm{d}\,\vec{n}(l)}{\mathrm{d}l}\right)^2 \mathrm{d}l = \frac{l_p}{2}\int_0^L \left(\frac{\mathrm{d}\theta(l)}{\mathrm{d}l}\right)^2 \mathrm{d}l \qquad (7)$$

where l_p is the effective persistence length of the bottle-brush backbone within the brush layer.

In the case of strong brush deformation, a section of the bottle-brush macromolecule forms an arch. The location of the turning point is determined by the condition $\mathrm{d}\theta(l)/\mathrm{d}l \approx 0$ (see Figure 8). Note that only a part of the bottle-brush between the grafting point and turning point provides the bending energy contribution balancing the compression stress. In order to estimate the bending energy contribution to brush compression, we can assume that the radius of curvature of an archlike bottle-brush section is on the order of $D/2$. The contour length of the section of the bottle-brush macromolecules forming an arc can be estimated as

$$\tilde{L} \approx \frac{\pi}{4} D \qquad (8)$$

The bending energy of the section of a bottle-brush macromolecule with contour length $\tilde{L}$ and having a radius of curvature $D/2$ is estimated as follows:

$$\frac{U_{\text{bend}}}{k_B T} \approx \frac{l_p}{2}\int_0^{\tilde{L}} \left(\frac{\mathrm{d}\theta(l)}{\mathrm{d}l}\right)^2 \mathrm{d}l \approx \frac{2 l_p \tilde{L}}{D^2} \approx \frac{l_p}{D} \qquad (9)$$

dx.doi.org/10.1021/la2018067 |*Langmuir* 2011, 27, 11044–11051

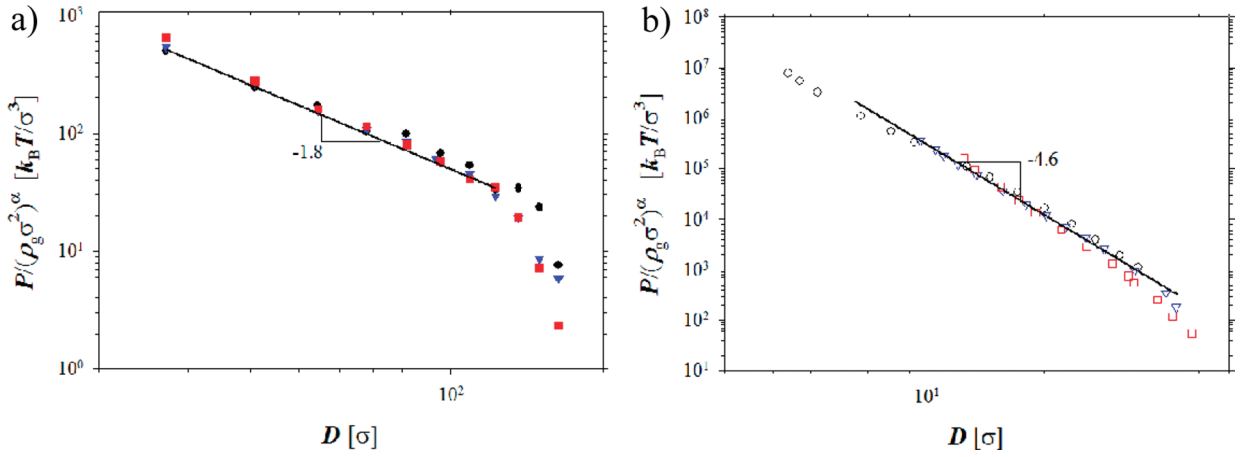

Figure 9. Dependence of disjoining pressure between (a) charged and (b) neutral bottle-brush layers at different brush grafting densities: (●, ○) $\rho_g = 1.24 \times 10^{-3}\,\sigma^{-2}$, (▼, ▽) $3.09 \times 10^{-3}\,\sigma^{-2}$, and (■, □) $4.43 \times 10^{-3}\,\sigma^{-2}$. The exponent was $\alpha = 1.5$ for charged systems and $\alpha = 2.4$ for neutral systems.

Here and below we will use a scaling analysis and neglect all numerical prefactors. The total energy of the bottle-brush layer is equal to the sum of the brush bending energy (eq 9) and the configurational entropy of osmotically active counterions[1−3] per bottle-brush macromolecule multiplied by the total number of bottle-brush chains, $S\rho_g$, within the brush area S:

$$\frac{U_{brush}}{k_BT} \approx S\rho_g\left[\frac{l_p}{D} + f^*mN_m \log\left(\sigma^3 f^* mN_m\rho_g/D\right)\right] \qquad (10)$$

where the second term in the brackets in eq 10 is the configurational entropy of the osmotically active counterions per bottle-brush chain and f^* is the fraction of osmotically active counterions. The disjoining pressure between two brush layers is obtained by differentiating eq 10 with respect to distance D between grafting surfaces:

$$P = -S^{-1}\frac{\partial U_{brush}}{\partial D} \propto \frac{k_BT\rho_g l_p}{D^2} + \frac{k_BT\rho_g f^* mN_m}{D} \qquad (11)$$

Our analysis of the counterion condensation in the bottle-brush layer shows that the fraction of free counterions f^* for these grafting densities is very small,[37] and thus interaction between two bottle-brush layers is dominated by the bending term:

$$P \propto \frac{k_BT\rho_g l_p}{D^2} \qquad (12)$$

This equation indicates that the observed $P \propto D^{-1.8}$ dependence of the disjoining pressure can be explained by the bending energy contribution of the compressed bottle-brush macromolecules. This also indicates a weak dependence of bottle-brush persistence length on the brush separation (see discussion below).

In the case of neutral brush layers, we see a much stronger dependence of disjoining pressure on substrate separation, $P \propto D^{-4.6}$ (see Figure 3). For dense neutral brush layers, the bottle-brush bending energy contribution has to be supplemented by the contribution due to excluded volume interactions between monomers. Close to the θ conditions for the polymer backbone, these interactions are dominated by three-body contacts. When this is taken into account, the disjoining pressure between two brush layers with average monomer density $\rho_m \approx \rho_g mN_m/D$ reduces to

$$P \propto \frac{k_BT\rho_g l_p}{D^2} + \frac{k_BT{\rho_g}^3\sigma^6(mN_m)^3}{D^3} \qquad (13)$$

The second term demonstrates stronger power law dependence on the separation D than the first term if one does not take into account dependence of the brush persistence length on brush separation. The bottle-brush persistence length can be estimated as $l_p \propto Ed^4/k_BT$,[39] where E is the Young's modulus of the bottle-brush and d is the bottle-brush diameter. For our brush grafting densities, $d \propto {\rho_g}^{-1/2}$ and the Young's modulus E is on the order of $E \propto \rho_m\partial P(\rho_m)/\partial\rho_m \approx k_BT\sigma^6(\rho_g mN_m/D)^3$, where we assumed that the pressure in overlapping brush layers is dominated by the three-body contacts, $P(\rho_m) \propto k_BT{\rho_m}^3\sigma^6$. Substituting dependence of the brush persistence length l_p on distance D and brush grafting density ρ_g, we can rewrite eq 13 as follows:

$$P \propto \frac{k_BT{\rho_g}^2\sigma^6(mN_m)^3}{D^5} + \frac{k_BT{\rho_g}^3\sigma^6(mN_m)^3}{D^3} \propto \frac{k_BT{\rho_g}^2\sigma^6(mN_m)^3}{D^5} \qquad (14)$$

This power law dependence of the disjoining pressure on substrate separation, $P \propto D^{-5}$, is close to the one observed in our simulations, $P \propto D^{-4.6}$.

In order to obtain the dependence of disjoining pressure P on brush grafting density, we have fitted simulation data shown in Figure 3 to a function $P \propto {\rho_g}^{\alpha}D^{-\beta}$. This procedure resulted in the following dependences of disjoining pressure P on brush grafting density and substrate separation:

$$P \propto {\rho_g}^{1.5\pm0.2}D^{-1.8\pm0.2} \quad \text{charged brush} \qquad (15a)$$

$$P \propto {\rho_g}^{2.4\pm0.2}D^{-4.6\pm0.3} \quad \text{neutral brush} \qquad (15b)$$

To assess the accuracy of the fitting procedure, we have collapsed simulation data for disjoining pressure between charged and neutral bottle-brush layers at different values of the brush grafting density by normalizing the pressure magnitude by ${\rho_g}^{1.5}$ and ${\rho_g}^{2.4}$ for charged and neutral bottle-brush layers, respectively. The results of this procedure are summarized in Figures 9 a and b. As one can see, the collapse of the data is reasonably good. It also

dx.doi.org/10.1021/la2018067 |Langmuir 2011, 27, 11044–11051

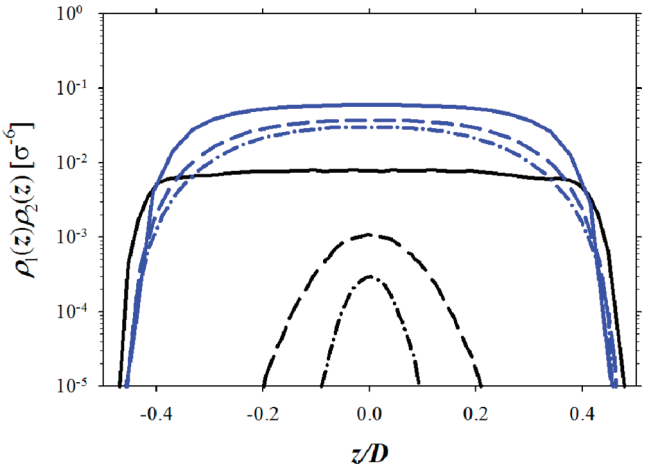

Figure 10. Dependence of the product $\rho_1(z)\rho_2(z)$ of monomer densities between substrates for (black) charged and (blue) neutral bottle-brush systems at brush grafting density $3.09 \times 10^{-3}\ \sigma^{-2}$ and at disjoining pressures P equal to (– · –) $1.2 \times 10^{-2}\ k_BT/\sigma^3$, (– – –) $2.3 \times 10^{-2}\ k_BT/\sigma^3$, and (—) $8.1 \times 10^{-2}\ k_BT/\sigma^3$. The corresponding distances between substrates D were equal to 93.2σ, 67.9σ, and 27.2σ for charged systems and 20.3σ, 18.0σ, and 13.4σ for neutral systems, respectively.

follows from eq 15b that our scaling expression for pressure P, eq 14, underestimates its dependence on the brush grafting density, with the difference between exponents on the order of 20%. Unfortunately, there is no simple procedure that will allow us to estimate the dependence of persistence length of charged bottle-brush macromolecules on brush compression and brush grafting density. Theoretical models of the electrostatic-induced chain bending rigidity[40−46] are limited to the case of a single chain (dilute solution regime), when interactions between charged monomers can be approximated by the Debye−Huckel potential. However, we can use eq 15a to evaluate the dependence of charged bottle-brush persistence length on brush grafting density. By comparing eqs 12 and 15a, we can establish that brush persistence length l_p scales with brush grafting density as $\rho_g^{1/2}$. A detailed study of the bottle-brush persistence length within brush layers and concentrated solutions will be a subject of separate publication.

To end this section, let us comment on the interpenetration between bottle-brush layers. The overlap between brush layers can be quantified by monitoring variation of the product $\rho_1(z)\rho_2(z)$ of the bottle-brush monomer densities from bottom, $\rho_1(z)$, and top, $\rho_2(z)$, substrates. In the region where two bottle-brush layers overlap, this quantity is nonzero. Figure 10 shows dependence of the product $\rho_1(z)\rho_2(z)$ for charged and neutral brush layers. For the same value of disjoining pressure, the charged bottle-brush layers are separated by larger distances and demonstrate weaker overlap manifested in smaller values at the maximum. Another interesting feature observed for charged brushes in comparison with neutral brush systems is the much flatter profile of the quantity $\rho_1(z)\rho_2(z)$ at $P = 8.1 \times 10^{-2}\ k_BT/\sigma^3$. This indicates almost uniform density distribution within strongly overlapped charged brush layers.

4. CONCLUSIONS

We have studied interactions between two substrates covered with charged and neutral bottle-brush macromolecules. Using molecular dynamics simulations and scaling analysis, we have established different scaling regimes in dependence of the disjoining pressure on substrate separation and bottle-brush grafting density. In the case of charged bottle-brushes, two brush layers begin to interact long before they physically overlap. In this regime, the interaction between two brush layers is due to diffusive counterion clouds that are formed outside the edges of the brush layers. At large separations, brush layers can be considered as charge surfaces with effective surface charge densities whose magnitude depends on the fraction of counterions condensed within the brush. The counterion density profile between two brush layers can be obtained by solving a one-dimensional nonlinear Poisson−Boltzmann equation for the slab geometry (see eq 5 and Figure 5). In the framework of this approach, there is a linear relationship between disjoining pressure and counterion concentration at the middle plane (see Figure 6).

In the interval of compressions where two brush layers begin to overlap, $D < 2H$, we observed a new universal scaling regime with $P \propto \rho_g^{1.5\pm0.2} D^{-1.8\pm0.2}$ for charged bottle-brush layers and $P \propto \rho_g^{2.4\pm0.2} D^{-4.6\pm0.3}$ for neutral bottle-brush layers (see Figure 9). This universal dependence of disjoining pressure on distance between brush-bearing substrates was attributed to a dominant contribution of the bending energy of the bottle-brush macromolecules to the interaction potential between brush layers. These scaling laws of disjoining pressure dependence on distance D between brush-bearing surfaces are qualitatively different from those observed for systems of charged and neutral brushes made of flexible linear chains. In the case of linear chains, excluded volume interactions between monomers and osmotic forces due to salt ions and counterions dominate the interactions between brush layers.[1−3]

It is important to point out the similarity between our result for charged bottle-brush systems and that obtained for compression of a brush made of charged semiflexible (DNA-like) chains.[47] Both systems demonstrate D^{-2} dependence of disjoining pressure on substrate separations. This should not be surprising because in both systems the bending energy contribution dominates the interactions between brush layers.

A model of interaction between two bottle-brush layers was recently proposed by Dean et al.[48] to explain experimental data on interactions between charged chondroitin sulfate glycosaminoglycan (CS-GAG) covered surfaces.[32,33] In the framework of this model,[48] the interaction between brushes is dominated by counterions and salt ions localized within brush layers, whose contributions to the layer interactions were taken into account in the framework of the Poisson−Boltzmann approach. This method was used to estimate interactions between layers by assuming the dominant contribution of interpenetration and compression deformation modes of the interacting brush layers. Our simulations have shown a qualitatively different picture of deformation of individual macromolecules within brush layers. According to our simulations, when two bottle-brush layers come into contact, the macromolecules forming these layers interpenetrate and bend at the same time. By bending, macromolecules minimize the interpenetration between layers. As we have shown, the bending energy contribution is a dominant term in the interaction energy between bottle-brush layers. This bottle-brush deformation mode was neglected in consideration by Dean et al.[48] The detailed comparison of our model with the nanomechanical measurements of interaction between CS-GAG covered substrates and investigation of the effect of salt concentration on these interactions will be subject of future publications.

AUTHOR INFORMATION

Corresponding Author
*E-mail: avd@ims.uconn.edu.

ACKNOWLEDGMENT

This work was supported by the National Science Foundation under Grant DMR-1004576.

REFERENCES

(1) Ruhe, J.; Ballauff, M.; Biesalski, M.; Dziezok, P.; Grohn, F.; Johannsmann, D.; Houbenov, N.; Hugenberg, N.; Konradi, R.; Minko, S.; et al. *Adv. Polym. Sci.* **2004**, *165*, 79–150.
(2) Netz, R. R.; Andelman, D. *Phys. Rep.* **2003**, *380*, 1–95.
(3) Ballauff, M.; Borisov, O. *Curr. Opin. Colloid Interface Sci.* **2006**, *11*, 316–323.
(4) Chen, M.; Briscoe, W. H.; Armes, S. P.; Klein, J. *Science* **2009**, *323*, 1698–1701.
(5) Claesson, P. M.; Poptoshev, E.; Blomberg, E.; Dedinaite, A. *Adv. Colloid Interface Sci.* **2005**, *114*, 173–187.
(6) Raviv, U.; Giasson, S.; Kampf, N.; Gohy, J. F.; Jerome, R.; Klein, J. *Nature* **2003**, *425*, 163–165.
(7) Klein, J.; Kumacheva, E.; Mahalu, D.; Perahia, D.; Fetters, L. J. *Nature* **1994**, *370*, 634–636.
(8) Lee, S.; Spencer, N. D. *Science* **2008**, *319*, 575–576.
(9) Ahrens, H.; Forster, S.; Hehn, C. A.; Kumar, N. A.; Naji, A.; Netz, R. R.; Seidel, C. *J. Phys. Chem. B* **2004**, *108*, 16870–16876.
(10) Currie, E. P. K.; Norde, W.; Stuart, M. A. C. *Adv. Colloid Interface Sci.* **2003**, *100*, 205–265.
(11) Pincus, P. *Macromolecules* **1991**, *24*, 2912–2919.
(12) Biesheuvel, P. M. *J. Colloid Interface Sci.* **2004**, *275*, 97–106.
(13) Pryamitsyn, V. A.; Leermakers, F. A. M.; Fleer, G. J.; Zhulina, E. B. *Macromolecules* **1996**, *29*, 8260–8270.
(14) Zhulina, E. B.; Birshtein, T. M.; Borisov, O. V. *Macromolecules* **1995**, *28*, 1491–1499.
(15) Zhulina, E. B.; Borisov, O. V. *J. Chem. Phys.* **1997**, *107*, 5952–5967.
(16) Binder, K. *Eur. Phys. J. E* **2002**, *9*, 293–298.
(17) Kumar, N. A.; Seidel, C. *Macromolecules* **2005**, *38*, 9341–9350.
(18) Kumar, N. A.; Seidel, C. *Phys. Rev. E* **2007**, *76*, No. 020801.
(19) Hehmeyer, O. J.; Stevens, M. J. *J. Chem. Phys.* **2005**, *122*, No. 134909.
(20) Hehmeyer, O. J.; Arya, G.; Panagiotopoulos, A. Z. *J. Chem. Phys.* **2007**, *126*, No. 244902.
(21) He, S. Z.; Merlitz, H.; Chen, L.; Sommer, J. U.; Wn, C. X. *Macromolecules* **2010**, *43*, 7845–7851.
(22) Seidel, C. *Macromolecules* **2003**, *36*, 2536–2543.
(23) Sandberg, D. J.; Carrillo, J. M. Y.; Dobrynin, A. V. *Langmuir* **2007**, *23*, 12716–12728.
(24) Carrillo, J. M. Y.; Dobrynin, A. V. *Langmuir* **2009**, *25*, 13158–13168.
(25) Tagliazucchi, M.; de la Cruz, M. O.; Szleifer, I. *Proc. Natl. Acad. Sci. U.S.A.* **2010**, *107*, 5300–5305.
(26) Klein, J.; Kumacheva, E.; Perahia, D.; Mahalu, D.; Warburg, S. *Faraday Discuss.* **1994**, *98*, 173–188.
(27) Muller, M. T.; Yan, X. P.; Lee, S. W.; Perry, S. S.; Spencer, N. D. *Macromolecules* **2005**, *38*, 5706–5713.
(28) Raviv, U.; Giasson, S.; Kampf, N.; Gohy, J. F.; Jerome, R.; Klein, J. *Langmuir* **2008**, *24*, 8678–8687.
(29) Klein, J. *Proc. IME Part J* **2006**, *220*, 691–710.
(30) Liberelle, B.; Giasson, S. *Langmuir* **2008**, *24*, 1550–1559.
(31) June, R. K.; Mejia, K. L.; Barone, J. R.; Fyhrie, D. P. *Osteoarthritis Cartilage* **2009**, *17*, 669–676.
(32) Dean, D.; Han, L.; Grodzinsky, A. J.; Ortiz, C. *J. Biomech.* **2006**, *39*, 2555–2565.
(33) Dean, D.; Han, L.; Ortiz, C.; Grodzinsky, A. J. *Macromolecules* **2005**, *38*, 4047–4049.
(34) Dunlop, I. E.; Briscoe, W. H.; Titmuss, S.; Jacobs, R. M. J.; Osborne, V. L.; Edmondson, S.; Huck, W. T. S.; Klein, J. *J. Phys. Chem. B* **2009**, *113*, 3947–3956.
(35) Frenkel, D.; Smit, B. *Understanding Molecular Simulations*; Academic Press: New York, 2002.
(36) Plimpton, S. *J. Comput. Phys.* **1995**, *117*, 1−19; lammps.sandia.gov.
(37) Carrillo, J. M. Y.; Dobrynin, A. V. *Langmuir* **2010**, *26*, 18374–18381.
(38) Safran, S. A. *Statistical Thermodynamics of Surfaces, Interfaces, and Membranes*; Westview Press: Boulder, CO, 2003.
(39) Landau, L. D.; Lifshitz, E. M. *Theory of Elasticity*. Pergamon Press: Oxford, U.K., 2000.
(40) Skolnick, J.; Fixman, M. *Macromolecules* **1977**, *10*, 944–948.
(41) Odijk, T. *J. Polym. Sci., Polym. Phys. Ed.* **1977**, *15*, 477–483.
(42) Barrat, J. L.; Joanny, J. F. *Europhys. Lett.* **1993**, *24*, 333–338.
(43) Netz, R. R.; Orland, H., V. *Eur. Phys. J. B* **1999**, *8*, 81–98.
(44) Dobrynin, A. V.; Rubinstein, M. *Prog. Polym. Sci.* **2005**, *30*, 1049–1118.
(45) Gubarev, A.; Carrillo, J. M. Y.; Dobrynin, A. V. *Macromolecules* **2009**, *42*, 5851–5860.
(46) Dobrynin, A. V.; Carrillo, J.-M. Y. *J. Phys. Condens. Matter* **2009**, *21*, No. 424112.
(47) Wynveen, A.; Likos, C. N. *Phys. Rev. E* **2009**, *80*, No. 010801(R).
(48) Dean, D.; Seog, J.; Ortiz, C.; Grodzinsky, A. J. *Langmuir* **2003**, *19*, 5526–5539.